Physics and Chemistry in Space 21
Space and Solar Physics

R. Schwenn E. Marsch (Eds.)

Physics of the Inner Heliosphere

2 Particles, Waves and Turbulence

Springer-Verlag

DOI: https://doi.org/10.1007/978-3-642-75364-0; Publisher: Springer-Verlag Berlin Heidelberg, 1991. Print ISBN: 978-3-642-75366-4; Online ISBN: 978-3-642-75364-0; Series Print ISSN: 0079-1938

9. Waves and Instabilities

Donald A. Gurnett

9.1 Introduction

It is widely recognized that even though the solar wind is essentially collisionless, to a good approximation it can be treated as a fluid. To understand this behavior, it is first necessary to understand the microscopic processes that control the macroscopic properties of the plasma. In a collisionless plasma such as the solar wind, it is now widely recognized that waves play a role similar to collisions in an ordinary fluid. As the plasma flows outward from the sun, dynamical changes cause the velocity distribution function to deviate from an equilibrium thermal distribution. In the absence of collisions these deviations continue to grow until the velocity-space gradients parallel and perpendicular to the magnetic field, $\partial f/\partial v_{\parallel}$ and $\partial f/\partial v_{\perp}$, become so large that plasma instabilities start to occur. These instabilities lead to the growth of waves. As the waves grow to large amplitudes, wave–particle interactions eventually act to eliminate the velocity-space gradients that cause the instability. Waves and instabilities thereby play a crucial role in preventing large deviations from thermal equilibrium. For a review of the types of plasma instabilities and wave–particle interactions that can occur in a plasma see, for example, Hasegawa [9.34], or Melrose [9.47].

For reference, the primary plasma wave modes of importance in the solar wind are summarized in Fig. 9.1, which shows a plot of the phase velocity, ω/k, as a function of frequency for typical solar wind conditions at 1 AU. To simplify the presentation, only waves propagating parallel to the magnetic field are shown. At low frequencies the relevant characteristic speeds of the plasma are the Alfvén speed, $V_A = B/\sqrt{\mu_0 \varrho_m}$, and the sound speed, $V_s = \sqrt{kT/m}$, where B is the magnetic field strength, ϱ_m is the mass density, T is the temperature, and m is the ion mass. Except very close to the sun the solar wind speed, V_{sw}, is substantially greater than either of these speeds.

At low frequencies three modes exist. These modes are called the fast, intermediate, and slow magnetohydrodynamic (MHD) waves. At higher frequencies these three modes merge into the whistler mode, the ion cyclotron mode, and the ion acoustic mode. The whistler mode has a resonance (point of zero phase velocity) at the electron cyclotron frequency, f_c^-, and the ion cyclotron mode has a resonance at the ion cyclotron frequency, f_c^+. The upper frequency limits of these two modes are at f_c^- and f_c^+, respectively. Both the whistler mode and the ion cyclotron mode are electromagnetic, since the waves have both electric

Physics and Chemistry in Space - Space and Solar Physics, Vol. 21
Physics of the Inner Heliosphere II Editors: R. Schwenn · E. Marsch
© Springer-Verlag Berlin Heidelberg 1991

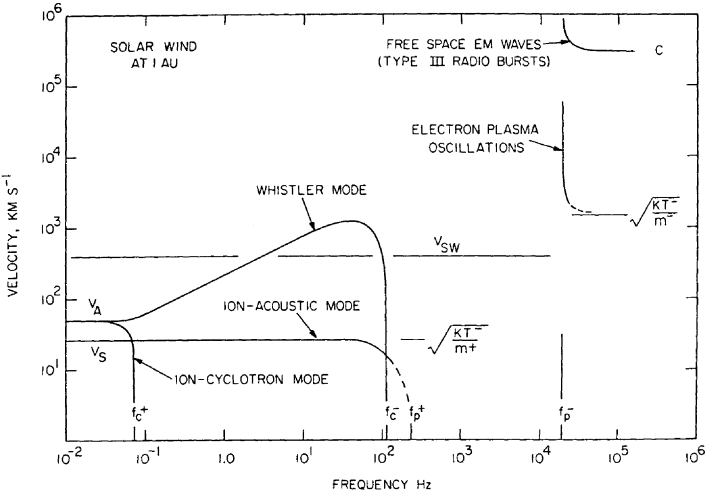

Fig. 9.1. A plot showing the phase velocity of selected plasma wave modes in the solar wind for propagation parallel to the magnetic field. Modes with phase velocities below the solar wind velocity, V_{sw}, are strongly Doppler shifted

and magnetic fields. These modes can be driven unstable by a variety of free energy sources, including currents, anisotropies and particle beams [9.47]. At frequencies above the ion cyclotron frequency the magnetic field of the ion acoustic mode becomes negligibly small compared to the electric field. This type of wave, with no magnetic field, is called an electrostatic wave, since the electric field can be derived from a potential. The ion acoustic mode has many properties similar to a sound wave in an ordinary gas and is strongly damped by Landau damping unless the electron temperature, T_e, is much greater than the ion temperature, T_i. The region of strong damping is indicated by a dashed line in Fig. 9.1. The upper frequency limit of the ion acoustic mode is the ion plasma frequency, f_p^+. If $T_e \gg T_i$, then the ion acoustic mode can be driven unstable by a number of free-energy sources, including currents [9.57], electron heat conduction [9.14], and ion beams [9.44].

At high frequencies, near the electron plasma frequency, f_p^-, three additional modes appear. Two of these modes are the free space electromagnetic modes, one of which is right-hand polarized, and the other of which is left-hand polarized. The phase velocities go to infinity as the wave frequency approaches f_p^-. At frequencies well above the plasma frequency the phase velocities of the two free space modes approach the speed of light, c. The free space modes do not propagate at frequencies below the electron plasma frequency.

Slightly above the plasma frequency a third purely electrostatic mode also occurs. This mode is called a Langmuir wave or an electron plasma oscillation. For phase velocities well above the electron thermal speed, the electron plasma oscillation represents an almost purely electrostatic oscillation at the electron

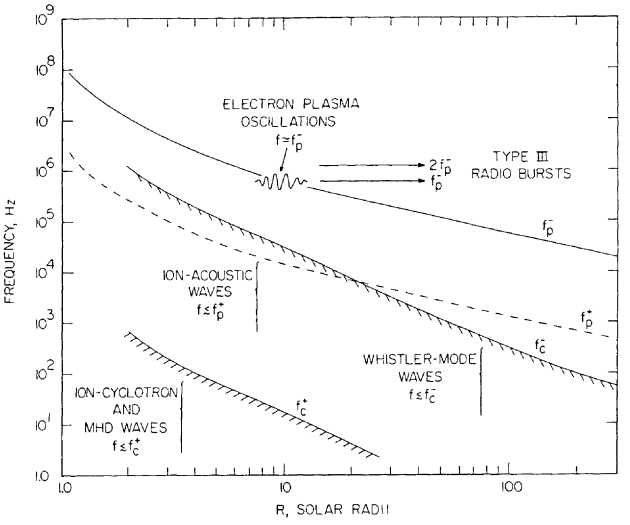

Fig. 9.2. The characteristic frequencies of the plasma as a function of radial distance from the sun

plasma frequency. As the phase velocity decreases, approaching the electron thermal speed, the frequency begins to increase. However, in this region the oscillations are strongly damped by Landau damping. The region of strong damping is indicated by a dashed line. Electron plasma oscillations are driven unstable whenever a region of positive slope, $\partial f/\partial v_{\|} > 0$, occurs in the electron distribution function. These distribution functions are characteristic of beams, such as those injected into the solar wind by solar flares [9.45].

When only small amplitude waves are considered, the two free space electromagnetic modes propagate completely independent of the other plasma wave modes. However, as the amplitude increases, nonlinear effects cause the two free space modes to be coupled to the plasma wave modes. Plasma waves can then transfer energy to the free space modes, thereby producing radio emissions that can be detected at large distances from the coupling region. This nonlinear mode conversion process is the mechanism by which most solar radio emissions detected at the earth are believed to be produced [9.42].

To illustrate the typical radial variations that occur in the solar wind, Fig. 9.2 shows the characteristic frequencies of the solar wind plasma as a function of heliocentric radial distance, R. At the orbit of the earth the electron plasma frequency is typically about 20 kHz, and the ion plasma frequency is about 450 Hz. The electron and ion cyclotron frequencies are typically about 140 Hz and 0.07 Hz, respectively. At large distances from the sun, where the solar wind velocity is essentially constant, conservation of particles implies that the solar wind electron density must vary as $1/R^2$. Since the electron plasma frequency depends on the square root of the electron density, $f_p^- = 9\sqrt{n_e}$ kHz, where n_e is in units of cm^{-3}, the electron plasma frequency must vary as $1/R$. As the

solar wind velocity decreases near the sun, the electron plasma frequency decreases more rapidly than $1/R$. The approximate radial variation based on existing models of the solar wind velocity [9.35] is shown in Fig. 9.2. The ion plasma frequency varies like the electron plasma frequency but for protons is a factor of $\sqrt{m^-/m^+} = \frac{1}{43}$ lower than the electron plasma frequency. The radial variations of the electron and ion cyclotron frequencies are more complicated since the magnetic field makes a transition from a radial, $1/R^2$, configuration to an Archimedian spiral, $1/R$, configuration near the earth's orbit. Near the sun even more complicated and less predictable variations, generally steeper than $1/R^2$, occur because of coronal loops and other complicated magnetic field structures. The radial variations of f_c^- and f_c^+ shown in Fig. 9.2 are based on magnetic field models discussed by Hundhausen [9.35]. The ion cyclotron frequency shown is for protons and is a factor of $m^-/m^+ = \frac{1}{1836}$ lower than the electron cyclotron frequency. Other ions, such as He^{++}, also exist in the solar wind. The cyclotron frequencies of these heavier ions, which are normally much less abundant than protons, are not shown.

For the purposes of this review, only waves with frequencies near and above the proton cyclotron frequency are considered. Waves and fluctuations at frequencies below the ion cyclotron frequency are normally studied by static-field magnetometers whose characteristics are quite different from instruments designed to detect plasma waves at frequencies above the ion cyclotron frequency. Numerous spacecraft have carried instruments to study plasma waves in the solar wind. These include *OGO 3* and *5*, *Pioneer 8* and *9*, *IMP 6*, *7* and *8*, *Hawkeye 1*, *Helios 1* and *2*, *ISEE 1*, *2* and *3*, and *Voyager 1* and *2*. Of these, only *Helios 1* and *2* provided measurements significantly inside of 1 AU. Except for *Voyager 1* and *2*, which provided measurements beyond 1 AU, the remaining spacecraft provided measurements near the earth's orbit. Since this review concentrates mainly on the inner heliosphere, inside of 1 AU, the results presented are mainly from *Helios 1* and *2*, although results from other spacecraft are discussed when appropriate.

The plasma wave instrumentation on *Helios 1* and *2* is typical of the types of instrumentation used to detect plasma waves in the solar wind. Two types of sensors are used, one to detect electric fields and the other to detect magnetic fields. The electric field sensor consists of an electric dipole antenna, 32 meters tip-to-tip, mounted perpendicular to the spacecraft spin axis as shown in Fig. 9.3. Electric fields are detected by measuring the voltage difference between the two antenna elements using a sensitive differential amplifier. For a description of the electric field sensor and associated instrumentation on *Helios*, see Gurnett et al. [9.27]. The magnetic field sensor consists of a triaxial search coil magnetometer mounted on the end of a boom as shown in Fig. 9.3. The search coil magnetometer consists of a high permeability iron rod wound with a large number of turns of fine wire. Magnetic fields are measured by detecting the voltage induced in the winding with a sensitive preamplifier. Since only time-varying magnetic fields cause an induced voltage, this type of magnetometer responds only to wave magnetic fields, and not to static fields. For a description of the search coil

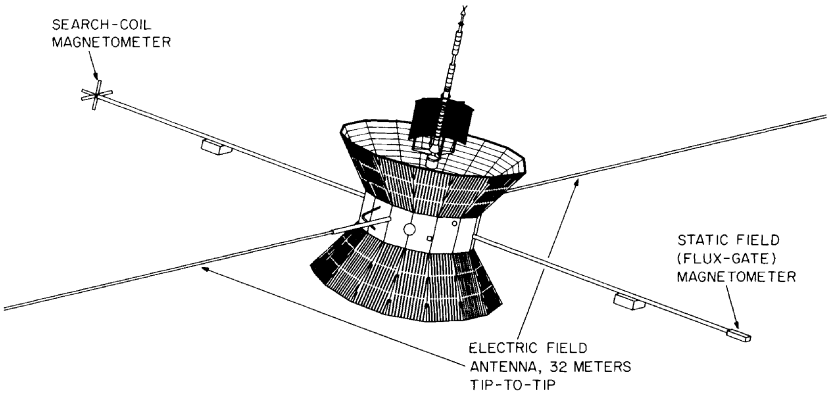

Fig. 9.3. A sketch of the *Helios* spacecraft showing the electric dipole antenna used for detecting wave electric fields and the search-coil magnetometer used for detecting wave magnetic fields

magnetometer and associated instrumentation on *Helios*, see Dehmel et al. [9.7], and Gliem et al. [9.22].

Since the types of plasma wave occurring in the solar wind are divided conveniently into electrostatic and electromagnetic waves, this review is organized by separately considering electrostatic and electromagnetic waves.

9.2 Electrostatic Waves

The *Helios* plasma wave instrument detected two primary types of electrostatic wave: electron plasma oscillations and ion acoustic waves. Examples of both types of wave are illustrated in Fig. 9.4 which shows a 16-channel plot of the electric field intensities detected by *Helios 2* at a heliocentric radial distance of 0.45 AU. The solid line in each frequency channel gives the peak electric field strength and the upper edge of the solid black band gives the average field strength. The time resolution for the peak and average field strength measurements varies with bit rate and in this case is 40 seconds. The electron plasma oscillations occur in the 56.2 kHz channel during the interval from about 0650 to 0740 UT, and the ion acoustic waves occur in the frequency range from about 1.0 to 17.8 kHz for the entire 8-hour duration of the plot. Because these two types of emission usually occur independently and have different characteristics, they will be discussed separately.

9.2.1 Electron Plasma Oscillations

Electron plasma oscillations are easily identified in the *Helios* electric field data because they usually occur in only one or two frequency channels near the local

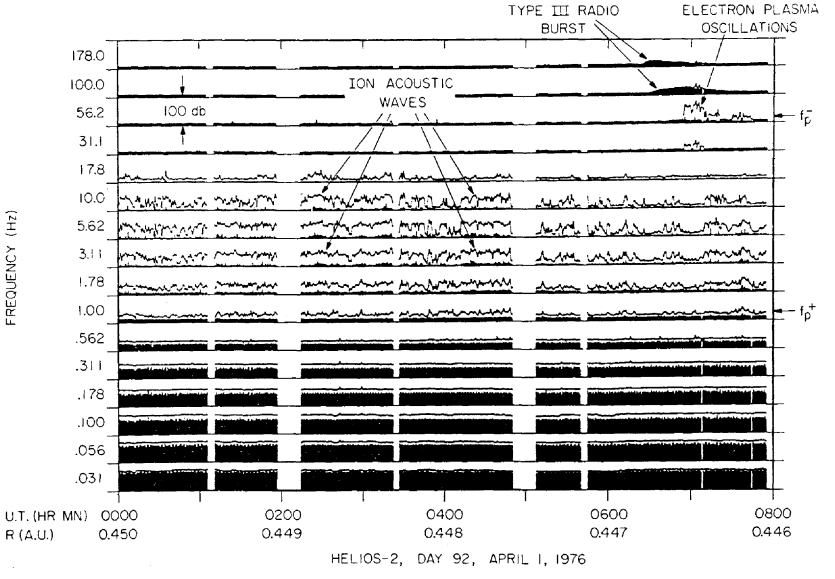

Fig. 9.4. A representative plot of the electric field intensities from *Helios 2* showing an electron plasma oscillation event associated with a type III solar radio burst and a period of enhanced ion acoustic wave activity

electron plasma frequency, f_p^-. Electron plasma oscillations are often associated with type III solar radio bursts of the type shown in Fig. 9.4, although they can also occur separately. Type III radio bursts are produced by flares and active regions on the sun and have a characteristic frequency–time variation, decreasing monotonically in frequency with increasing time [9.59]. The *Helios* observations of electron plasma oscillations occurring in association with type III radio bursts [9.24] confirm a long-standing theory for the origin of these radio bursts. According to this theory, first proposed by Ginzburg and Zheleznakov [9.21], the generation of type III radio bursts is a two-step process in which (1) electron plasma oscillations are first produced by energetic electrons from a solar flare, and (2) the energy in the plasma oscillations is converted to electromagnetic radiation via coupling to the free space electromagnetic modes. Because electrons are impulsively released by the flare, a beam-like region of positive slope, $\partial f/\partial v_\parallel > 0$, is generated near the leading edge of the energetic electron stream owing to time-of-flight considerations. The temporal evolution of the reduced one-dimensional distribution function, $f(v_\parallel)$, is illustrated in Fig. 9.5 for an electron plasma oscillation event detected by the *ISEE 3* spacecraft at 1 AU [9.45]. Since the growth rate of the plasma oscillations is proportional to $\partial f/\partial v_\parallel$ [9.57, 41], waves are only generated during the interval when $\partial f/\partial v_\parallel$ is positive. This interval is usually about 1 hour at 1 AU, decreasing to about 20 minutes at 0.3 AU. Because the region of positive slope is only present near the leading edge of the electron stream, the plasma oscillations are confined to a localized region that moves outward from the sun at a speed comparable to the energetic

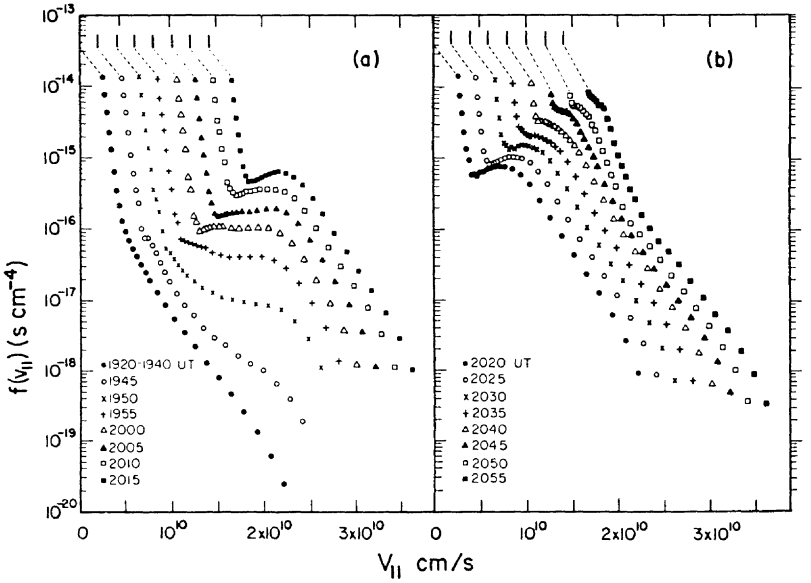

Fig. 9.5a,b. A sequence of reduced one-dimensional electron distribution functions from *ISEE 3* [9.45] showing energetic electrons arriving from a solar flare. Electron plasma oscillations occur during the times when the distribution function has a region of positive slope, $\partial f/\partial v_{||} > 0$

electron stream, typically $0.1c$ to $0.5c$. As the region of intense plasma oscillations moves outward from the sun, electromagnetic radiation is generated at f_p^- and $2f_p^-$, producing the decreasing emission frequency with increasing time that is characteristic of type III radio bursts. This radio emission process is illustrated in Fig. 9.2. At low frequencies, below about 1 MHz, the strongest radiation is usually at the second harmonic, $2f_p^-$, [9.11, 36, 28], although evidence also exists for radiation at the fundamental [9.37, 38]. Because the electromagnetic radiation propagates freely away from the source, the type III radiation is typically detected 10 to 20 minutes before the region of intense plasma oscillations arrives at the spacecraft.

By using a large number of electron plasma oscillation events detected over a several-year period, the variation of the electric field strength of the plasma oscillations can be determined as a function of radial distance from the sun [9.29, 32]. This variation is shown in Fig. 9.6. As can be seen, the electric field strength tends to decrease with increasing heliocentric radial distance, varying approximately as $R^{-1.4\pm0.5}$. This decrease is expected because the electric field to plasma energy density ratio, $E^2/8\pi nkT$, which controls the saturation intensity, is approximately constant. Since the number density n varies as R^{-2} and the temperature T varies as $R^{-2/7}$ [9.35], for a constant energy density ratio, the maximum electric field E is expected to vary approximately as $R^{-8/7}$. The observed radial variation is seen to be reasonably consistent with the expected radial variation. Typical maximum values for $E^2/8\pi nkT$ are about 2×10^{-5}.

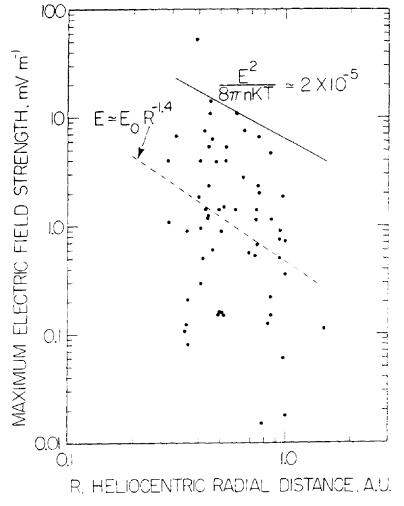

Fig. 9.6. The electric field strength of plasma oscillation events detected by *Helios 1* and *2* in association with type III radio bursts. The best-fit power law through these points varies as $R^{-1.4\pm0.5}$. The *solid line* shows the electric field intensity corresponding to an electric field to plasma energy density ratio of $E^2/8\pi nkT \simeq 2 \times 10^{-5}$

The radial variation of the field strength of the plasma oscillations can also be compared with the emissivity of the type III radiation, which varies as approximately R^{-6} [9.58]. For second-harmonic emission mechanisms, the emissivity should vary as E^4. This dependence occurs because the radiating current at the second harmonic is proportional to the product of the field strength of two interacting plasma oscillations. Since the power radiated is proportional to the square of the current, a fourth-power dependence on the electric field strength is expected. Since the emissivity varies approximately as R^{-6}, the electric field intensity should then vary as $R^{-1.5}$. This radial variation is seen to be in reasonable quantitative agreement with the observed radial variation.

High-time-resolution measurements of electron plasma oscillations detected by *Helios* [9.25] show that the electric field intensity is very spiky, with rapid intensity variations down to the time resolution of the instrument, which is about 50 ms. This very spiky electric field structure accounts for the very large peak to average field strength ratios evident in Fig. 9.4. Consideration of the nonlinear effects that stabilize the electron beam has led a number of investigators to predict that the electric field structure should be very spiky [9.52, 17, 2, 51, 50, 15, 23]. The origin of the spiky structure involves a focusing effect that causes the plasma oscillation intensity to increase in regions of decreased plasma density. If the wave intensity becomes sufficiently large, the electric field pressure causes the plasma density to decrease, further increasing the focusing and eventually forming a soliton-like structure that collapses down to a spatial scale of only a few Debye lengths. Collapsed plasma oscillation structures of this type, sometimes referred to as "spiky turbulence", have been observed in the laboratory [9.60]. For the receiver averaging time constant of the *Helios* instrument, $\sim$ 50 msec, it is not possible to resolve intensity fluctuations at the time scales, hundreds

of μs, required to resolve soliton-like structures. The maximum plasma oscillation field strengths measured by *Helios*, typically only 5 to 10 mV/m, are too small to reach the threshold electric field strength, $E^2/8\pi nkT \gtrsim (k\lambda_D)^2 \simeq 10^{-2}$ to 10^{-3}, required for soliton collapse. However, because of the relatively long, 50 ms, averaging interval, it is possible that field strengths much larger than 5 to 10 mV/m could be occurring on short time scales. Evidence of soliton-like intensity fluctuation has been reported by Gurnett et al. [9.33] for electron plasma oscillations detected in the solar wind upstream of Jupiter's bow shock.

9.2.2 Ion Acoustic Waves

The second basic type of electrostatic noise detected in the solar wind by *Helios* is a band of sporadic emissions between the proton and electron plasma frequency, f_p^+ and f_p^-. Because of the frequency range involved, these emissions were initially referred to as $f_p^+ < f < f_p^-$ noise [9.25]. In their initial interpretation of this noise, Gurnett and Anderson [9.25] suggested that the emissions are ion acoustic waves which are Doppler shifted into the frequency range $f_p^+ < f < f_p^-$ by the motion of the solar wind. As will be discussed shortly, considerable evidence now exists that these waves are ion acoustic waves, or a closely related ion-acoustic-like mode. For this reason, we will refer to the emissions as ion acoustic waves.

A typical example of the ion acoustic waves detected by *Helios* is shown in Fig. 9.4. The noise does not occur continuously but rather in episodes lasting for periods ranging from a few hours to several days. Episodes of enhanced ion acoustic wave activity usually occur a few times per month and tend to be more frequent and more intense closer to the sun. Periods of enhanced ion acoustic wave activity often recur on successive solar rotations, particularly ahead of high-speed solar wind streams [9.31] and in association with interplanetary shocks [9.30, 40]. An example of an ion acoustic wave event associated with an interplanetary shock is shown in Fig. 9.7. The ratio of the peak to average electric field strength is usually very large, typically greater than 40 dB, indicating that the noise is impulsive and sporadic on time scales of a few seconds or less. When the intensities are averaged over several minutes the spectrum appears very broad, usually extending from near f_p^+ to slightly below f_p^-. The cutoffs at f_p^+ and f_p^- are not rigid cutoffs, and, as will be discussed shortly, it is probably coincidental that the spectrum falls in this frequency range. As shown by Gurnett and Frank [9.26] and Gurnett et al. [9.31] both the intensity and frequency of the noise tend to increase with decreasing radial distance. This tendency is illustrated in Fig. 9.8, which shows representative electric field spectrums of the ion acoustic noise at three heliocentric radial distances: 1.73 AU from *Voyager 1*, 0.98 AU from *Helios 1*, and 0.47 AU from *Helios 1*. A statistical study of the radial dependence shows that the broad-band electric field strength varies approximately as $1/R$, varying from about 1 mV/m (10% quartile) at 0.33 AU to about 0.3 mV/m at 1 AU. Although *Helios* had no capability for obtaining electric field waveforms, wide-band measurements from *Voyager 2* [9.43] show that the ion acoustic waves

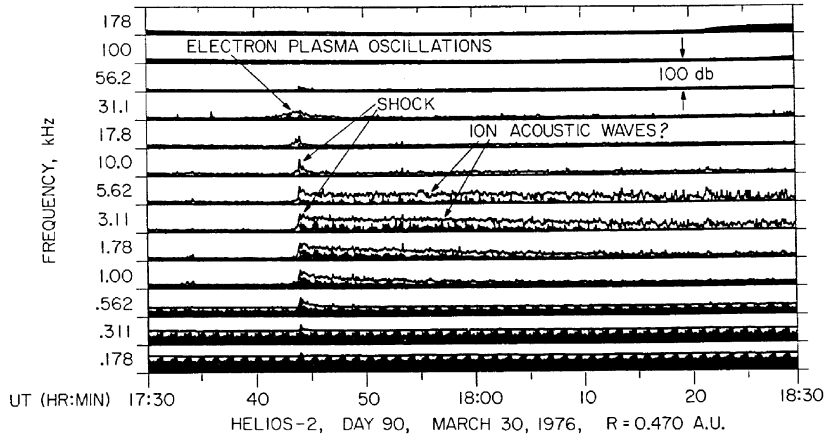

Fig. 9.7. An example of an ion acoustic wave event detected by *Helios 2* in association with an interplanetary shock. A region of weak electron plasma oscillations also occurs near the shock. For an analysis of this event, see Gurnett et al. [9.30]

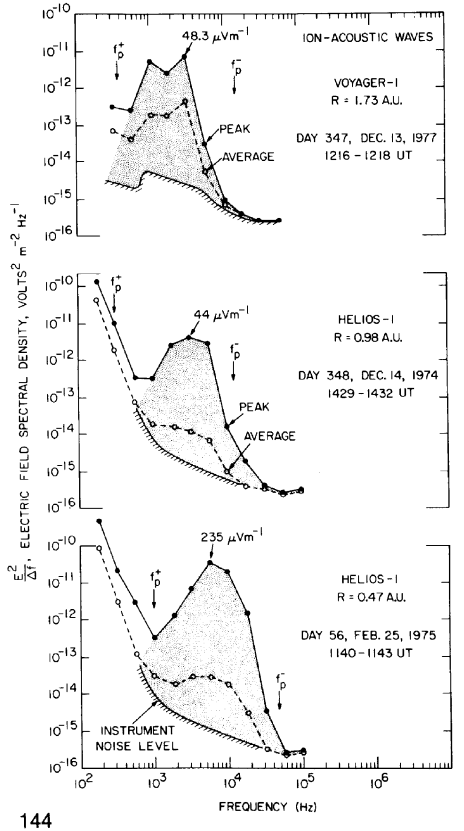

Fig. 9.8. Peak and average electric field spectral densities for ion acoustic waves at three representative radial distances from the sun. The spectrum increases in intensity and moves to higher frequencies with decreasing radial distance, usually staying in the range $f_p^+ < f < f_p^-$

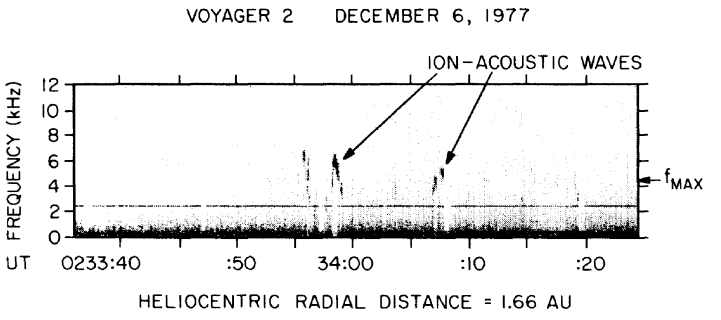

Fig. 9.9. A high-resolution frequency–time spectrogram of ion acoustic waves detected by *Voyager 2* at 1.66 AU. The ion acoustic emissions consist of a nearly monochromatic tone with a rapidly varying center frequency

consist of nearly monochromatic emissions whose center frequencies vary over a wide range on a time scale of a few seconds. A typical high-resolution frequency–time spectrogram of a burst of ion acoustic waves detected by *Voyager 2* is shown in Fig. 9.9. Because of rapid fluctuations in the center frequency of the emission, the spectrum appears to be very broad when averaged over longer intervals, as in Fig. 9.8, even though it is nearly monochromatic on short time scales.

The evidence that the $f_p^+ < f < f_p^-$ noise detected by *Helios* is caused by ion acoustic waves is somewhat indirect and is based mainly on comparisons with very similar waves observed upstream of the earth's bow shock. Because ion acoustic waves have very short wavelengths, the Doppler shift caused by the motion of the solar wind is substantial. When the Doppler shift is included, the frequency of an ion acoustic wave in the spacecraft frame of rest is given by

$$\omega = \frac{C_S k}{\sqrt{1 + k^2 \lambda_D^2}} + V_{sw} k \cos \theta_{kv} , \tag{9.1}$$

where $C_S = \sqrt{kT_e/m_i}$ is the ion acoustic speed, k is the wave number, θ_{vk} is the angle between the wave vector and the solar wind velocity, and λ_D is the Debye length. The rest-frame frequency of the ion acoustic wave is given by the first term, and the Doppler shift is given by the second term. For typical solar wind parameters, the Doppler shift is much larger than the rest-frame frequency. Therefore, to a good approximation $\omega \simeq V_{sw} k \cos \theta_{kv}$. Because of the onset of strong Landau damping at short wavelengths, k has a maximum value of $k\lambda_D \simeq 1$. The maximum frequency is then given by $\omega_{max} = V_{sw}/\lambda_D$. For typical solar wind parameters at 1 AU ($n = 5$ cm^{-3}, $T = 1.5 \times 10^5$ K, $V_{sw} = 400$ km/s) the maximum frequency is approximately $f_{max} \simeq 8.0$ kHz, which is in good agreement with the observed upper frequency limit (see Fig. 9.8). Since the electron temperature is nearly independent of radial distance [9.35] and since both V_{sw}/λ_D and f_p^- vary as the square root of the electron density, it is easy to verify that f_{max} is proportional to f_p^-. This relationship explains why the frequency of the ion acoustic waves appears to vary in direct proportion to f_p^- (see Fig. 9.8).

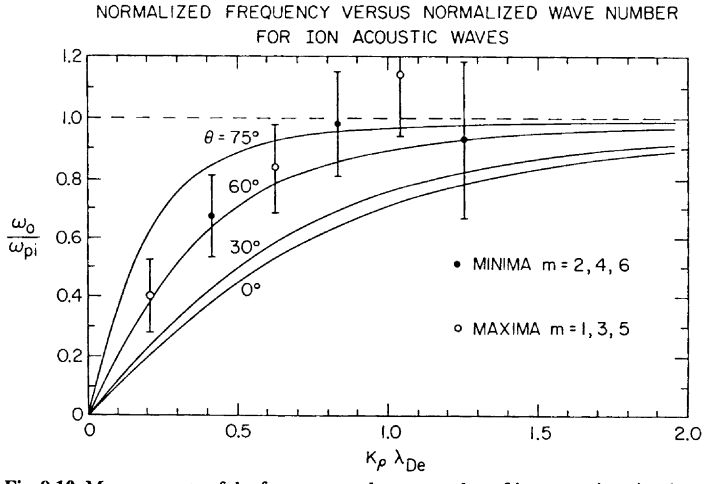

Fig. 9.10. Measurements of the frequency and wave number of ion acoustic noise detected by *ISEE 1* upstream of the earth's bow shock. The *solid curves* show the dispersion relation for the ion acoustic mode as a function of the polar angle θ of the wave vector, which is unknown

However, in this interpretation the upper cutoff frequency actually has no direct relationship to f_p^-. It is only coincidental that f_{max} is near f_p^-.

Although the upper cutoff frequency of the $f_p^+ < f < f_p^-$ noise is consistent with an ion acoustic wave interpretation, it does not uniquely identify the mode because other short wavelength modes also exist with cutoffs near $k\lambda_D \simeq 1$. These modes would also have an upper frequency cutoff at $\omega_{max} = V_{sw}/\lambda_D$. The evidence that the noise is due to ion acoustic waves rests on other observations. First, a well-known characteristic of the ion acoustic mode is that the damping is very sensitive to the electron to ion temperature ratio, T_e/T_i. Ion acoustic waves are weakly damped if $T_e/T_i \gg 1$, and strongly damped if $T_e/T_i = 1$. Using solar wind plasma measurements from *Helios*, Gurnett et al. [9.31] have shown that the electric field intensity of the $f_p^+ < f < f_p^-$ noise increases as T_e/T_i increases, as would be expected for an ion acoustic instability. Second, Gurnett and Frank [9.26] have pointed out that the ion acoustic noise detected by *Helios* has essentially identical characteristics to a band of low-frequency electric field noise detected upstream of the earth's bow shock between about 1 to 10 kHz. By using techniques not available on *Helios*, Fuselier and Gurnett [9.16] have been able to measure the wavelength of the waves. By independently measuring both the wavelength and the frequency, the dispersion relation can be determined. An example of such dispersion-relation measurements is shown in Fig. 9.10. Although the polar angle θ of the wave vector is a free parameter, the basic shape of the dispersion curve, including the break at $k\lambda_{De} \simeq 1$, and the upper frequency limit at ω_{pi}, is in excellent agreement with the ion acoustic dispersion relation. Although these measurement are not available on *Helios*, they strongly suggest that the waves detected by *Helios* are also ion acoustic waves.

Given that the waves detected by *Helios* are ion acoustic waves, the question arises as to how these waves are generated. This is a difficult question that has not been completely answered. Upstream of the earth's bow shock it is now well established [9.54, 26, 1] that the comparable types of waves are closely associated with energetic, 1 to 10 keV, proton beams arriving from the bow shock. Since ion acoustic waves are also observed ahead of interplanetary shocks [9.40], one might think that the ion acoustic waves detected by *Helios* far from the earth are produced by an ion beam in the solar wind. In fact, Lemons et al. [9.44], have suggested that the waves are produced by an ion-beam instability. Despite the reasonableness of this line of argument, to date no definite relationship has been established between ion beams in the interplanetary medium and ion acoustic waves. This situation is in part due to the absence of suitable energetic ion measurements on *Helios*. However, attempts to establish a relationship using the more comprehensive ion measurements available on *ISEE 3* at 1 AU have also not been successful. Finally, it should be pointed out that energetic protons with energies of 1 to 10 keV have velocities too high to resonate with the ion acoustic mode. Therefore, it is unlikely that these ions are the direct source of excitation of the ion acoustic waves, if indeed they are ion acoustic waves.

Many years ago, even before the discovery of the solar wind ion acoustic waves, it was suggested by Forslund [9.14] that the conduction of heat away from the sun could excite ion acoustic waves in the solar wind. This instability occurs because if no net current is allowed to flow in the plasma then the presence of a third moment (heat flux) in the electron distribution function produces a shift between the peaks of the electron and ion distribution functions. If the heat flux is sufficiently large, this shift produces a double hump in the reduced distribution function that makes the ion acoustic mode unstable. Comparative studies of the *Helios* plasma and plasma wave data [9.31] show that the ion acoustic wave intensities are closely correlated with the electron heat flux. This correlation is shown in Fig. 9.11. Detailed studies of electron and ion distribution functions by Dum et al. [9.10] also show that the electron heat flux can account for the ion acoustic waves observed by *Helios*. The electron heat flux instability therefore seems to provide the most reasonable basis for understanding how these waves are generated. However, there are still unresolved difficulties. In some cases ion acoustic waves are observed when T_e/T_i is near one. Under these conditions the ion acoustic mode should be strongly damped. Also, in a few of the cases analyzed by Dum et al. [9.10] the ion acoustic mode was found to be stable even though waves were present. The origin of the instability under these unusual conditions remains unresolved. Marsch and Chang [9.46] have suggested that under these conditions another instability involving lower hybrid waves may be required to explain the noise.

The possible macroscopic consequences of the solar wind ion acoustic waves detected by *Helios* has not been established. Forslund [9.14] suggested that ion acoustic waves in the solar wind could have important consequences for controlling heat conduction in the solar wind. Usually the ion acoustic waves detected by *Helios* are very weak. The ratio of the electric field energy density to the plasma

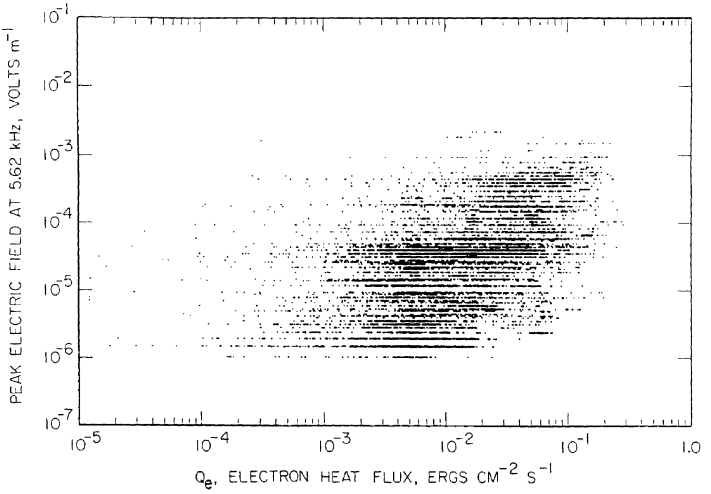

Fig. 9.11. A plot of simultaneous measurements of the electric field intensity of ion acoustic waves and the electron heat flux. The field intensity clearly tends to increase as the heat flux increases, suggesting that the ion acoustic waves may be driven by an electron heat-flux instability

energy density, $E^2/8\pi nkT$, is only about 10^{-5} to 10^{-7} during intense bursts, and much smaller on the average. Whether such low intensities can have significant macroscopic effects on the solar wind has not been adequately explored.

9.3 Electromagnetic Waves

Three primary types of electromagnetic waves are observed in the solar wind: MHD waves, ion cyclotron waves, and whistler-mode waves. Since electromagnetic waves always have a magnetic field component, these waves can be most easily identified by using magnetic field measurements. As can be seen from Fig. 9.1, at 1 AU MHD waves and ion cyclotron waves occur at frequencies below 10^{-1} Hz, in the frequency range where static-field magnetometers provide the best sensitivity. Whistler-mode waves on the other hand occur at much higher frequencies, up to 10^2 Hz, in the frequency range where search-coil magnetometers provide the best sensitivity. Therefore, both types of measurements must be used to study the spectrums of these waves.

9.3.1 MHD Waves and Ion Cyclotron Waves

An example of a magnetic field spectrum obtained by combining measurements from a static-field (flux-gate) magnetometer and a search-coil magnetometer is shown in Fig. 9.12 (from Denskat et al. [9.9]). These data were obtained from *Helios 2* at a radial distance of 0.30 AU. The magnetic field spectral densities

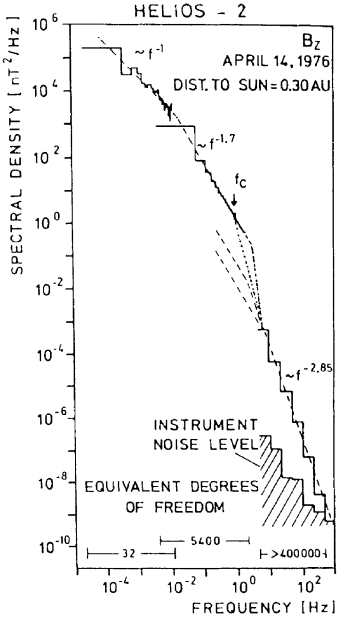

Fig. 9.12. A representative magnetic field spectrum from *Helios 2* at 0.3 AU. The abrupt decrease in amplitude at about 2 Hz is believed to be due to cyclotron damping of electromagnetic ion cyclotron waves propagating outward from the sun. The spectrum above 2 Hz is mainly due to whistler-mode noise

below 2 Hz were computed by performing a power spectral analysis of a time series of flux-gate magnetometer measurements. The magnetic field spectral densities at frequencies above 4.7 Hz were obtained using a set of eight bandpass filters from the search-coil magnetometer.

As can be seen, the spectrum decreases monotonically with increasing frequencies, varying approximately as $f^{-1.55}$ at low frequencies, steepening to approximately $f^{-2.9}$ at high frequencies. A discontinuity, or inflection point, in the spectrum occurs from 2 Hz to 4.7 Hz. This portion of the spectrum is shown by dashed lines in Fig. 9.12. Although the inflection point corresponds almost exactly to the gap between the two instruments, Denskat et al. [9.9] argue that the effect is real and is caused by a change in the plasma wave spectrum. Further evidence for an important change in the spectrum in this frequency range is given by the slope, which shifts from a $f^{-1.7}$ variation below 2 Hz to a $f^{-2.8}$ variation above 4.7 Hz.

In the frequency range around a few Hz, the only resonance or propagation cutoff that could account for a change in the spectrum is the proton cyclotron frequency. The measured proton cyclotron frequency, f_c^+, is indicated in Fig. 9.12. As can be seen, the proton cyclotron frequency is near, but somewhat below, the point where the inflection occurs in the spectrum. This offset is believed to be caused by a Doppler shift. Because the solar wind is moving relative to the spacecraft, the frequency, f', detected in the spacecraft frame of reference is shifted from the rest frame frequency, f, by the Doppler effect. The frequency

in the spacecraft frame of reference is given by

$$f' = f\left[1 + (V_{sw}/V_p)\cos\,\theta_{kv}\right]\ , \tag{9.2}$$

where V_p is the phase velocity and θ_{kv} is the angle between the solar wind velocity and the direction of propagation. Since the solar wind velocity is typically a factor of five or more greater than the phase velocity of the ion cyclotron mode, the Doppler shift could be easily a factor of five, or more. Doppler shifts of this magnitude could easily explain the offset between the inflection point in the spectrum and the proton cyclotron frequency. The offset is positive, toward higher frequencies, for waves propagating away from the sun ($\theta_{kv} < 90°$).

Next we consider the origin of the MHD waves. For many years [9.5, 6] it has been known that intense low-frequency MHD wave fluctuations exist in the solar wind. These waves propagate outward from the sun, apparently originating from turbulent solar wind heating processes in the solar corona. The intense low-frequency magnetic field fluctuations in Fig. 9.12 are caused by these waves. These fluctuations are probably a superposition of the fast, intermediate and slow MHD waves described in the introduction. Unfortunately, the three MHD wave modes cannot be uniquely resolved by measurements from a single spacecraft. Therefore, the exact distribution of wave energy between the three modes is not known. For a review of the observations and their interpretation, see Barnes [9.3]. Usually, it is assumed that some energy exists in the MHD mode that connects to the ion cyclotron mode. As the waves propagate outward from the sun the ion cyclotron frequency gradually decreases (see Fig. 9.1). As the ion cyclotron frequency approaches the wave frequency, the waves are strongly damped by ion cyclotron damping. This damping eventually absorbs all of the energy in the ion cyclotron mode. Denskat et al. [9.9] propose that absorption of wave energy by cyclotron damping causes the abrupt decrease in the magnetic field spectral density near the ion cyclotron frequency. Studies of the spatial variation in the magnetic field fluctuations by Denskat and Neubauer [9.8] show that the fluctuations decrease rapidly with increasing radial distance from the sun, as would be expected if the waves are being absorbed.

9.3.2 Whistler-Mode Waves

It is evident from the magnetic field spectrum in Fig. 9.12 that a significant amount of wave energy extends up to frequencies as high as 300 Hz, above the proton cyclotron frequency. These frequencies are much too high to be propagating in the ion cyclotron mode. Since the ion acoustic mode is electrostatic and has no magnetic field, the only electromagnetic mode that can account for magnetic field fluctuations in this frequency range is the whistler mode. For this reason Denskat et al. [9.9] conclude that this turbulence must consist of whistler-mode waves.

Whistler-mode turbulence comparable to that shown in Fig. 9.12 is observed at all heliocentric radial distances sampled by *Helios 1* and *2*, and appears to

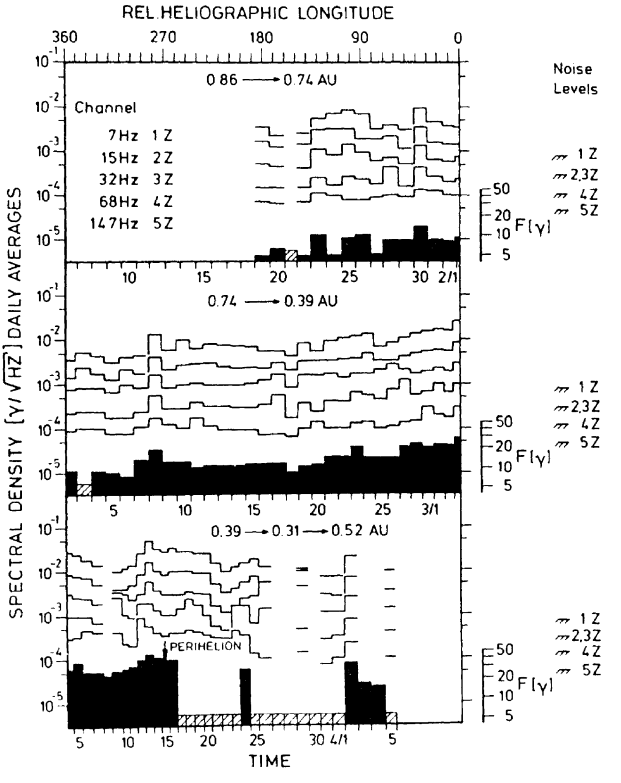

Fig. 9.13. Representative whistler-mode magnetic field intensities for a *Helios 1* pass from 0.86 to 0.31 AU. Note the increase in intensity as the spacecraft approaches closer to the sun

be a permanent feature of the solar wind plasma. Figure 9.13 shows a plot of daily averages of the magnetic field intensities in five frequency channels (7 Hz to 147 Hz) for a period in which *Helios 1* covers the radial distance range from near aphelion (0.86 AU) to perihelion (0.31 AU). These frequency channels all respond exclusively to the whistler-mode portion of the solar wind magnetic field spectrum. As can be seen, substantial fluctuations in the whistler-mode magnetic field intensities occur from day to day. However, a general trend can also be seen for the intensities to increase with decreasing heliocentric radial distance. This trend, for the whistler-mode intensities to increase closer to the sun, has been confirmed on a statistical basis by Beinroth and Neubauer [9.4] using several years of data from *Helios 1* and *2*.

Enhanced whistler-mode wave intensities are also observed in association with interplanetary shocks. Figure 9.14 shows the magnetic field intensities in eight channels from 6.8 Hz to 1.47 kHz for an interplanetary shock that occurred on 30 March 1976. This is the same shock that was described earlier in the

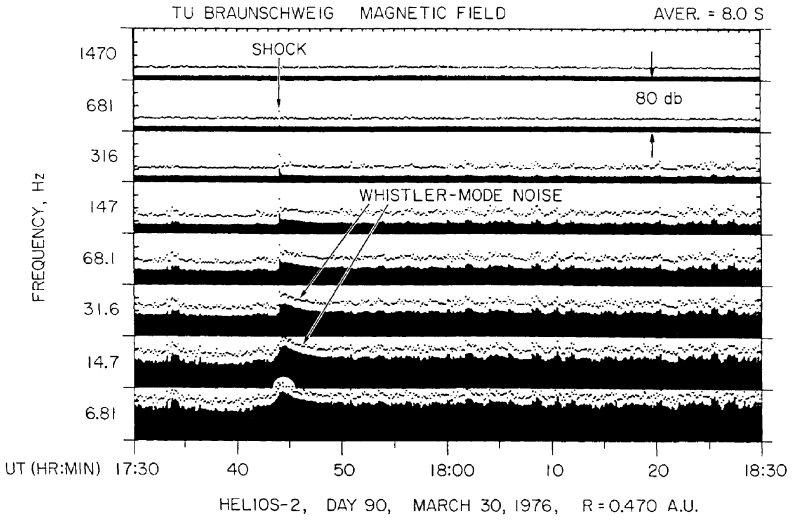

Fig. 9.14. Whistler-mode magnetic field intensities associated with an interplanetary shock. Note the abrupt burst of noise at the shock, followed by a gradual decrease in intensity downstream of the shock

section on ion acoustic waves. As can be seen, a very strong enhancement of the magnetic noise intensities occurs at the shock, lasting for several minutes downstream of the shock. The magnetic noise in this case actually starts to increase several seconds before the magnetic field ramp associated with the shock. Representative spectrums of the whistler-mode magnetic field intensities in the precursor region immediately ahead of the shock, at the shock, and in the wake region downstream of the shock are shown in Fig. 9.15. For a further analysis of this shock, see Gurnett et al. [9.30]. These magnetic field intensities are typical of the other shocks detected by *Helios*.

Short bursts of whistler-mode noise have also been observed in association with other types of discontinuities in the solar wind. These include tangential discontinuities, rotational discontinuities, and reversible magnetic field variation. For a discussion of these events, see Neubauer et al. [9.49]. In some of these cases the whistler-mode noise is produced by instabilities generated in the current sheet associated with the discontinuity, whereas in others the discontinuity itself may act to duct the waves to the spacecraft from a distant source.

Although it is possible that the background of whistler- mode noise in the solar wind may be propagating outward from a source near the sun, the occurrence of enhanced whistler-mode intensities at shocks and other local discontinuities demonstrates that a local whistler-mode instability must be operative in the solar wind. As discussed by Kennel and Petschek [9.39] a Doppler-shifted cyclotron resonance interaction provides the most likely mechanism for converting free energy in the particle distribution into the whistler-mode waves. The normal cyclotron resonance interaction of whistler-mode waves is with electrons, since

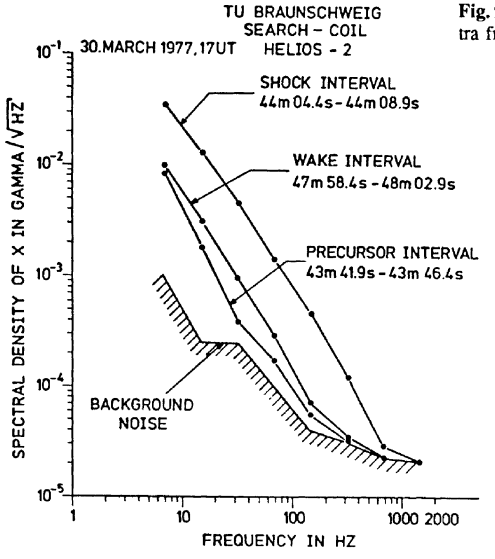

Fig. 9.15. Representative magnetic field spectra from the shock shown in Fig. 9.14

both the waves and electrons rotate in the right-hand sense with respect to the static magnetic field. However, whistler-mode waves can also resonate with ions if the component of particle velocity along the magnetic field, $v_{\|}$, exceeds the parallel component of the phase velocity, $\omega/k_{\|}$. This type of interaction is called the anomalous cyclotron resonance.

A wide variety of free energy sources can give rise to whistler-mode wave growth via cyclotron resonance interactions. For the normal cyclotron resonance interaction, electron anisotropies with perpendicular temperature greater than the parallel temperature, $T_{\perp} > T_{\|}$, provide a well-known free energy source for producing whistler-mode noise. This free energy source occurs whenever a loss-cone is present and is responsible for the intense whistler-mode noise commonly observed in planetary magnetospheres. However, in the solar wind the plasma expands into a region of decreasing magnetic field, which because of conservation of the first adiabatic invariant tends to make $T_{\|} > T_{\perp}$, thereby inhibiting the loss-cone type of instability. When $T_{\|} > T_{\perp}$, the ions have the proper anisotropy to produce whistler-mode wave growth via the anomalous cyclotron resonance interaction [9.53, 20].

Other free energy sources that could produce whistler-mode waves via a cyclotron resonance interaction include currents and the electron heat flux. Except for certain isolated conditions that occur near magnetic field discontinuities, currents are not expected to be an important source of whistler-mode noise. However, the electron heat flux remains a viable possibility. As discussed by Feldman et al. [9.12], the electron heat flux produces a shift between the velocities of the cool "core" electron distribution and the hot "halo" electron distribution. Gary et al. [9.18, 19] have shown that this shift can lead to the growth of whistler-mode

waves in the solar wind. Feldman et al. [9.13] have further examined various correlations that exist in the solar wind electron data and suggest that whistler-mode waves driven by the electron heat flux may play an important role in regulating the electron heat flux in the solar wind. At the present time, no clear consensus has emerged as to which of these processes is responsible for the whistler-mode noise in the solar wind. For further comments on the theoretical considerations involved, see Schwartz [9.56].

9.4 Conclusion

In this paper we have reviewed the basic characteristics of plasma waves in the inner heliosphere, with particular emphasis on the results from *Helios 1* and *2*. Of the various observations presented, the tendency for wave intensities to increase with decreasing radial distance from the sun is particularly striking. Electric field measurements show that both the intensity and frequency of occurrence of electrostatic ion acoustic waves and electron plasma oscillations increase rapidly with decreasing heliocentric radial distance. Magnetic field measurements also show that the intensity of the electromagnetic ion cyclotron and whistler-mode turbulence increases rapidly with decreasing radial distance from the sun.

The general tendency for plasma wave intensities to increase near the sun is also confirmed by the *Voyagers 1* and *2* measurements beyond 1 AU. As discussed by Gurnett et al. [9.29], Kurth et al. [9.43], and Scarf et al. [9.55], the intensities of electron plasma oscillations, ion acoustic waves, and type III solar radio bursts all decrease rapidly with increasing heliocentric radial distance. In fact, beyond about 2 AU, solar wind plasma waves are seldom detected by *Voyager*. Even at the orbit of the earth, some of these waves, such as the electron plasma oscillations associated with type III radio bursts, are very rare and seldom detectable.

Although the precise reasons for the strong radial dependence has not been analyzed in detail, the fundamental principles involved are obvious. As described in Sect. 9.1, plasma instabilities are driven by deviations from thermal equilibrium. Since the strongest spatial gradients occur in the region near the sun, and since the sun provides the source of the deviations from thermal equilibrium, it is to be expected that the strongest wave intensities should be observed near the sun. What is not presently understood is the role of the observed waves in determining the steady-state properties of the solar wind. Future theoretical effort is needed to understand the effect of plasma waves on the equilibrium state of the solar wind. Considerable room also exists for improvements in the observations. *Helios 1* and *2* only provided measurements over a little more than a factor of three in heliocentric radial distance. Given the rapid increase in plasma wave intensities as one proceeds from 1.0 to 0.29 AU, one naturally wonders how much stronger the plasma wave intensities become closer to the sun. The answer will have to await future missions that approach closer to the sun, such as the solar probe that is currently being studied.

Acknowledgements. The research at the University of Iowa has been supported by NASA through contract NAS5-11279 with Goddard Space Flight Center and grant NAGW-1488 with NASA Headquarters.

References

9.1 Anderson, R.R., C.C. Harvey, M.M. Hoppe, B.T. Tsurutani, T.E. Eastman, J. Etcheto, Plasma waves near the magnetopause, J. Geophys. Res., **87**, 2087, 1982.

9.2 Bardwell, S., M.V. Goldman, Three-dimensional Langmuir wave instabilities in type III solar radio bursts, Astrophys. J., **209**, 912, 1976.

9.3 Barnes, A., Hydromagnetic waves and turbulence in the solar wind, *Solar System Plasma Physics,* Vol. 1, ed. by E.N. Parker, C.F. Kennel, and L.J. Lanzerotti, North-Holland, Amsterdam, 249, 1979.

9.4 Beinroth, H.J., F.M. Neubauer, Properties of whistler-mode waves from 0.3 and 1.0 AU from Helios observations, J. Geophys. Res., **86**, 7755, 1981.

9.5 Coleman, P.J., Jr., Hydromagnetic waves in the interplanetary plasma, Phys. Rev. Lett., 17, 207, 1966.

9.6 Coleman, P.J., Jr., Turbulence, viscosity, and dissipation in the solar wind plasma, Astrophys. J., **153**, 371, 1968.

9.7 Dehmel, G., F.M. Neubauer, D. Lukoschus, J. Wawretzko, E. Lammers, Das Induktionsspulen-Magnetometer-Experiment (E4), Raumfahrtforschung, **19**, 241, 1975.

9.8 Denskat, K.U., F.M. Neubauer, Statistical properties of low-frequency magnetic fluctuations in the solar wind from 0.29 to 1.0 AU during solar minimum conditions: Helios 1 and 2, J. Geophys. Res., **87**, 2215, 1982.

9.9 Denskat, K.U., H.J. Beinroth, F.M. Neubauer, Interplanetary magnetic field power spectra with frequencies from 2.4 x 10-5 Hz to 470 Hz from Helios-observations during solar minimum conditions, J. Geophys. Res., **54**, 60, 1983.

9.10 Dum, C.T., E. Marsch, W. Pilipp, D.A. Gurnett, Ion sound turbulence in the solar wind, in *Solar Wind Four,* ed. by H. Rosenbauer, Max-Planck-Institut Report MPAE W100-81-31, Lindau, Germany, 299, 1981.

9.11 Fainberg, J., R.G. Stone, Satellite observations of type III solar radio bursts at low frequencies, Space Sci. Rev., **16**, 145, 1974.

9.12 Feldman, W.C., J.R. Asbridge, S.J. Bame, M.D. Montgomery, S.P. Gary, Solar wind electrons, J. Geophys. Res., **80**, 4181, 1975.

9.13 Feldman, W.C., J.R. Asbridge, S.J. Bame, S.P. Gary, M.D. Montgomery, Electron parameter correlations in high-speed streams and heat flux instabilities, J. Geophys. Res., **81**, 2377, 1976.

9.14 Forslund, D.S., Instabilities associated with heat conduction in the solar wind and their consequences, J. Geophys. Res., **75**, 17, 1970.

9.15 Freud, H.P., K. Papadopoulos, Oscillating two-stream and parametric decay instability in a weakly magnetized plasma, Phys. Fluids, **23**, 139, 1980.

9.16 Fuselier, S.A., D.A. Gurnett, Short wavelength ion waves upstream of the Earth's bow shock, J. Geophys. Res., **89**, 91, 1984.

9.17 Galeev, A.A., R.Z. Sagdeev, Yu.S. Sigov, V.D. Shapiro, V.I. Shevchenko, Nonlinear theory for the modulation instability of plasma waves, Sov. J. Plasma Phys. Engl. Transl., **1**, 5, 1975.

9.18 Gary, S.P., W.C. Feldman, D.W. Forslund, M.D. Montgomery, Electron heat flux instabilities in the solar wind, Geophys. Res. Lett., **2**, 79, 1975a.

9.19 Gary, S.P., W.C. Feldman, D.W. Forslund, M.D. Montgomery, Heat flux instabilities in the solar wind, J. Geophys. Res., **80**, 4197, 1975b.

9.20 Gary, S.P., M.D. Montgomery, W.C. Feldman, D.W. Forslund, Proton temperature anisotrophy instabilities in the solar wind, J. Geophys. Res., **81**, 1241, 1976.

9.21 Ginzburg, V.L., V.V. Zheleznyakov, On the possible mechanism of sporadic radio emission (radiation in an isotropic plasma), Sov. Astron., **AJ 2**, 653, 1958.

9.22 Gliem, F., G. Dehmel, G. Musmann, C. Turke, U. Krupstedt, R.P. Kugel, Die Bordrechner der Helios-Magnetometer- Experiment E2 and E4, Raumfahrtforschung, **20**, 16, 1976.

9.23 Goldman, M.V., G.F. Reiter, D.R. Nicholson, Radiation from a strongly turbulent plasma: Application to electron beam-excited solar emission, Phys. Fluids, **23**, 388, 1980.

9.24 Gurnett, D.A., R.R. Anderson, Electron plasma oscillations associated with type III radio bursts, Science, **194**, 1159, 1976.
9.25 Gurnett, D.A., R.R. Anderson, Plasma wave electric fields in the solar wind: Initial results from Helios 1, J. Geophys. Res., **82**, 632, 1977.
9.26 Gurnett, D.A., L.A. Frank, Ion acoustic waves in the solar wind, J. Geophys. Res., **83**, 58, 1978.
9.27 Gurnett, D.A., R.R. Anderson, D.L. Odem, The University of Iowa, HELIOS solar wind plasma wave experiment, [E5a], Raumfahrtforschung, **5**, 245, 1975.
9.28 Gurnett, D.A., M.M. Baumback, H. Rosenbauer, Stereoscopic direction finding analysis of a type III solar radio burst: Evidence for emission at 2fp-, J. Geophys. Res., **83**, 616, 1978.
9.29 Gurnett, D.A., R.R. Anderson, F.L. Scarf, W.S. Kurth, The heliocentric radial variation of plasma oscillations associated with type III radio bursts, J. Geophys. Res., **83**, 4147, 1978.
9.30 Gurnett, D.A., F.M. Neubauer, R. Schwenn, Plasma wave turbulence associated with an interplanetary shock, J. Geophys. Res., **84**, 541, 1979.
9.31 Gurnett, D.A., E. Marsch, W. Pilipp, R. Schwenn, H. Rosenbauer, Ion acoustic waves and related plasma observations in the solar wind, J. Geophys. Res., **84**, 2029, 1979.
9.32 Gurnett, D.A., R.R. Anderson, R.L. Tokar, Plasma oscillations and the emissivity of type III radio bursts, in *Radio Physics of the Sun*, ed. by M. Kundu and T. Gergely, IAU, 369, 1980.
9.33 Gurnett, D.A., J.E. Maggs, D.L. Gallagher, W.S. Kurth, F.L. Scarf, Parametric interaction and spatial collapse of beam-driven Langmuir waves in the solar wind, J. Geophys. Res., **86**, 8833, 1981.
9.34 Hasegawa, A., *Plasma Instabilities and Nonlinear Effects*, Springer-Verlag, Berlin, Heidelberg, New York, 1975.
9.35 Hundhausen, A.J., *Coronal Expansion and Solar Wind*, Springer-Verlag, Berlin, Heidelberg, New York, 1972.
9.36 Kaiser, M.L., The solar elongation distribution of low frequency radio bursts, Solar Physics, **45**, 181, 1975.
9.37 Kellogg, P.J., Fundamental emission in three type III solar bursts, Astrophys. J., **236**, 696, 1980.
9.38 Kellogg, P.J., Observations concerning the generation and propagation of type III solar bursts, Astron. Astrophys., **169**, 329, 1986.
9.39 Kennel, C.F., H.E. Petschek, Limit on stably trapped particle fluxes, J. Geophys. Res., **71**, 1–28, 1966.
9.40 Kennel, C.F., F.L. Scarf, F.V. Coroniti, E.J. Smith, D.A. Gurnett, J. Geophys. Res., **87**, 17, 1982.
9.41 Krall, N.A., A.W. Trivelpiece, *Principles of Plasma Physics*, McGraw-Hill, 1973.
9.42 Kundu, M.R., *Solar Radio Astronomy*, Interscience, New York, 1965.
9.43 Kurth, W.S., D.A. Gurnett, F.L. Scarf, High-resolution spectrograms of ion acoustic waves in the solar wind, J. Geophys. Res., **84**, 3413, 1979.
9.44 Lemons, D.S., J.R. Asbridge, S.J. Bame, W.C. Feldman, S.P. Gary, J.T. Gosling, The source of electrostatic fluctuations in the solar wind, J. Geophys. Res., **84**, 2135, 1979.
9.45 Lin, R.P., D.W. Potter, D.A. Gurnett, F.L. Scarf, Energetic electrons and plasma waves associated with a solar type III radio burst, Astrophys. J., **251**, 364, 1981.
9.46 Marsch, E., T. Chang, Lower hybrid waves in the solar wind, J. Geophys. Res., **88**, 6869, 1983.
9.47 Melrose, D.B., *Instabilities in Space and Laboratory Plasmas*, Cambridge University Press, Cambridge, 1986.
9.48 Musmann, G., F.M. Neubauer, A. Maier, E. Lammers, Das Förstersonden-Magneticfeld-experiment (E2), Raumfahrtforschung, **19**, 232, 1975.
9.49 Neubauer, F.M., G. Musmann, G. Dehmel, Fast magnetic fluctuations in the solar wind: Helios 1, J. Geophys. Res., **82**, 3201, 1977.
9.50 Nicholson, D.R., M.V. Goldman, P. Hoyng, J.S. Weatherall, Nonlinear langmuir waves during type III solar radio bursts, Ap. J., **223**, 605, 1978.
9.51 Papadopoulos, K., On the physics of strong turbulence for electron plasma waves, *Proc. Varenna School on Plasma Physics*, Pergamon, New York, 355, 1978.
9.52 Papadopoulos, K., M.L. Goldstein, R.A. Smith, Stabilization of electron streams in the type III solar radio bursts, Astrophys. J., **190**, 175, 1974.
9.53 Scarf, F.L., J.H. Wolfe, R.W. Silva, A plasma instability associated with thermal anisotropies in the solar wind, J. Geophys. Res., **72**, 993, 1967.

9.54 Scarf, F.L., R.W. Fredricks, L.A. Frank, C.T. Russell, P.J. Coleman, Jr., M. Neugebauer, Direct correlations of large amplitude waves with suprathermal protons in the upstream solar wind, J. Geophys. Res., **75**, 7316, 1970.

9.55 Scarf, F.L., E. Marsch, W. Pilipp, D.A. Gurnett, Ion sound turbulence in the solar wind, in *Solar Wind Four*, ed. by H. Rosenbauer, Max-Planck-Institut Report MPAE W100-81-31, Lindau, Germany, 299, 1981.

9.56 Schwartz, S.J., Plasma instabilities in the solar wind: A theoretical review, Rev. Geophys. and Space Phys., **18**, 313, 1980.

9.57 Stix, T., *The Theory of Plasma Waves*, McGraw-Hill, New York, 1962.

9.58 Tokar, R.L., D.A. Gurnett, The volume emissivity of type III radio bursts, J. Geophys. Res., **85**, 2353, 1980.

9.59 Wild, J.P., Observations of the spectrum of high- intensity solar radiation at meter wavelengths, Aust. J. Sci. Res., **3**, 541, 1950.

9.60 Wong, A.Y., B.H. Quon, Spatial collapse of beam-driven plasma waves, Phys. Rev. Lett., **34**, 1499, 1975.